ACCOUNTS
of chemical research

Tuning the Topology and Functionality of Metal–Organic Frameworks by Ligand Design

DAN ZHAO,[†] DAREN J. TIMMONS,[‡] DAQIANG YUAN,[†] AND HONG-CAI ZHOU*,[†]

[†]*Department of Chemistry, Texas A&M University, College Station, Texas 77842, United States, and* [‡]*Department of Chemistry, Virginia Military Institute, Lexington, Virginia 24450, United States*

RECEIVED ON AUGUST 10, 2010

CONSPECTUS

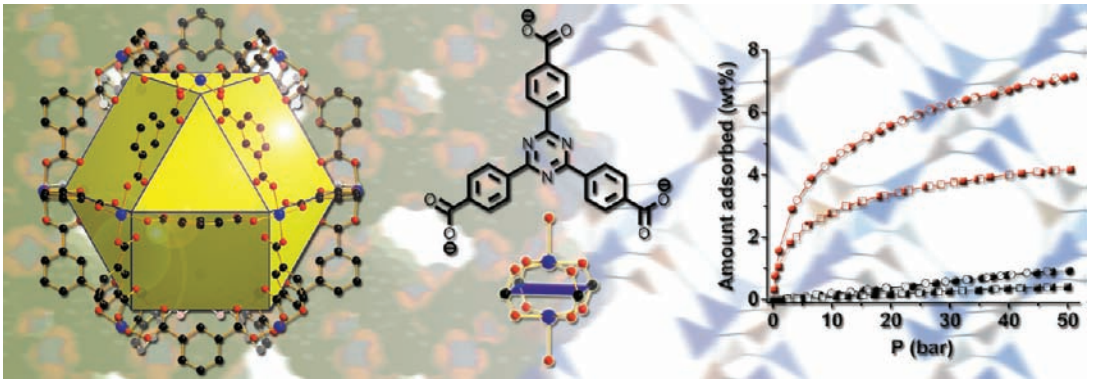

Metal–organic frameworks (MOFs)—highly crystalline hybrid materials that combine metal ions with rigid organic ligands—have emerged as an important class of porous materials. The organic ligands add flexibility and diversity to the chemical structures and functions of these materials. In this Account, we summarize our laboratory's experience in tuning the topology and functionality of MOFs by ligand design.

These investigations have led to new materials with interesting properties. By using a ligand that can adopt different symmetry conformations through free internal bond rotation, we have obtained two MOFs that are supramolecular stereoisomers of each other at different reaction temperatures. In another case, where the dimerized ligands function as a D_3-Piedfort unit spacer, we achieve chiral (10,3)-a networks.

In the design of MOF-based materials for hydrogen and methane storage, we focused on increasing the gas affinity of frameworks by using ligands with different geometries to control the pore size and effectively introduce unsaturated metal centers (UMCs) into the framework. Framework interpenetration in PCN-6 (PCN stands for porous coordination network) can lead to higher hydrogen uptake. Because of the proper alignment of the UMCs, PCN-12 holds the record for uptake of hydrogen at 77 K/760 Torr. In the case of methane storage, PCN-14 with anthracene-derived ligand achieves breakthrough storage capacity, at a level 28% higher than the U.S. Department of Energy target.

Selective gas adsorption requires a pore size comparable to that of the target gas molecules; therefore, we use bulky ligands and network interpenetration to reduce the pore size. In addition, with the help of an amphiphilic ligand, we were able to use temperature to continuously change pore size in a 2D layer MOF. Adding charge to an organic ligand can also stabilize frameworks. By ionizing the amine group within mesoMOF-1, the resulting electronic repulsion keeps the network from collapsing, giving rise to the first case of mesoporous MOF that demonstrates the type IV isotherm. We use dendritic hexacarboxylate ligands to synthesize an isoreticular series of MOFs with (3,24)-connected network topology. The cuboctahedral cages serve as building blocks that narrow the opening of the mesocavities into microwindows and stabilize these MOFs. The resulting materials have exceptionally high surface areas and hydrogen uptake capacities.

Despite the many achievements in MOF development, there is still ample opportunity for further exploration. We will be continuing our efforts and look forward to contributing to this blossoming field in the next decade.

Published on the Web 12/02/2010 www.pubs.acs.org/accounts
10.1021/ar100112y

1. Introduction

The study of metal−organic frameworks (MOFs) is developing nearly explosively, as indicated by the skyrocketing growth in the number of MOF publications and the number of MOF structures determined in the past decade. Possessing the merits of both organic and inorganic building units, MOFs can fill a niche in the search for new porous materials.[1,2] The use of the reticular approach—the recognition that the pairing of certain geometric building blocks has predictable outcomes—has greatly facilitated the intentional construction of MOFs with certain geometries.[3,4] Despite all the progress and promise, developing the synthetic control required for the intentional 3D arrangement of atoms still remains a Holy Grail in crystal engineering and materials chemistry.

This Account summarizes our work in the MOF field with specific focus on tuning the topology and functionality of MOFs by ligand design. While the rationalization of the MOF topology is commonly based on metal cluster secondary building units (SBUs, shown in Figure 1),[5] which are always generated in situ, the arbitrariness of these SBUs under various synthetic conditions limits their utility in topological prediction. On the contrary, most of the organic ligands preformed in MOF synthesis are normally robust in the assembly procedure. The geometric predictability of organic ligands makes them excellent building blocks for MOF design. It is the combination of both inorganic SBUs and organic ligands that determines the final frameworks' topologies. A library of cross-coupling reactions such as Suzuki coupling, Sonogashira coupling, and Buchwald−Hartwig amination reaction facilitates the ligand design and preparation.[6] Ligand design can be used not only to enrich the diversity of MOF topology, to study supramolecular isomerism such as interpenetration, symmetry-preserved isomerization, and conformation fixation, but also to modify the functionality of MOFs for specific applications such as gas storage and gas separation.

2. Design and Synthesis Strategy

2.1. Ligand Design. Some of the carboxylate ligands used in our group are shown in Chart 1 and have been designed with an eye toward synthetic convenience and ease of crystallization. They range from ditopic to hexatopic, display different geometry and length, and contain different functional groups. Such a rich ligand library gives us the opportunity to systematically study the relationship between the geometry of the ligand and the functionality of the generated network.

2.2. Network Synthesis. Solvothermal reactions have proven to be an effective synthetic approach for the formation of 3D networks with high crystallinity. These high quality crystals are needed for structure determination enabling an exploration of their inner space. A routine solvothermal reaction procedure involves loading ligands, metal salts, and solvents in thick-wall glass tubes, sealing the tubes under vacuum after flash freezing, and heating at elevated temperatures. With the proper conditions and good geometry match between the ligands and metal ions, crystalline products will form within several days. The nature of the solvothermal synthesis is actually a Lewis acid−base reaction, in which the deprotonated ligands act as Lewis bases while the metal ions serve as the Lewis acids. If the reaction goes too quickly, bulk precipitation occurs instead of the growth of single crystals. Modifying the reaction conditions so that the rate of ligand deprotonation matches that of the coordination bond formation is crucial. Solvents such as dimethyl formamide (DMF), diethyl formamide (DEF), and dimethyl acetamide (DMA) tend to undergo hydrolysis at elevated temperatures (60−85 °C), releasing amines capable of deprotonating the carboxylic acid ligands and facilitating the reaction. Without being hydrolyzed, dimethyl sulfoxide (DMSO) can be used at higher temperature conditions (100 °C or above), which helps to overcome the energy barrier and generate products with novel geometry. If necessary, the pH and polarity of the reaction media can be adjusted by adding inorganic acid or mixing in additional solvents. There is no universal reaction condition incorporating all ligands and metal ions, and different conditions are required for specific ligand and metal ion combinations. It is here that experience and serendipity combine to give success.

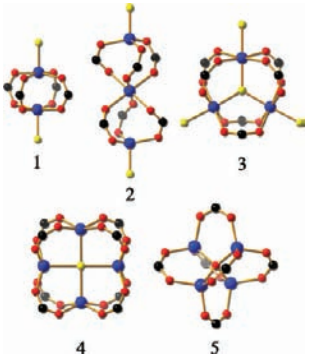

FIGURE 1. Commonly encountered secondary building units (SBUs) (black, carbon; red, oxygen; blue, metal; yellow, others. Similar hereinafter): (1) dinuclear paddlewheel; (2) trinuclear hourglass; (3) trinuclear prism; (4) tetranuclear cuboid; (5) tetranuclear octahedron.

3. Supramolecular Isomerism

Supramolecular isomerism and polymorphism in coordination polymer systems are very common and have been studied for a long time.[7] In principle, ligand stereoisomerism, which stems from conformation change, will give rise to

CHART 1. Selected Carboxylate Ligands Used in Zhou's Group

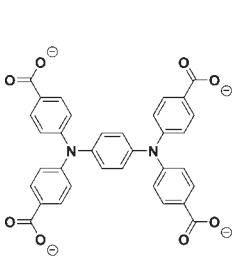

1, tcppda

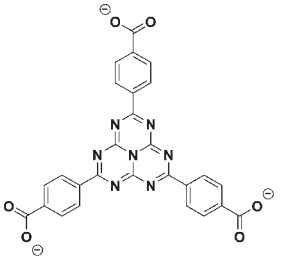

2, htb

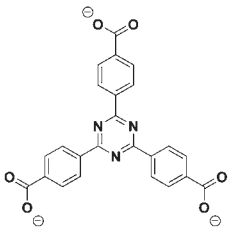

3, tatb

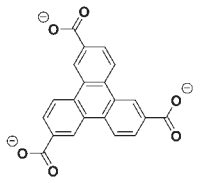

4, ttca

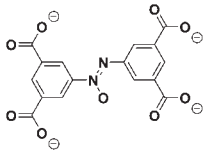

5, aobtc

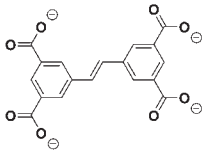

6, sbtc

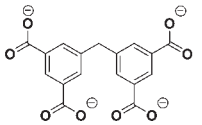

7, mdip

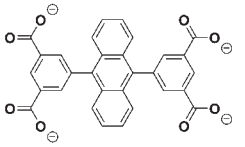

8, adip

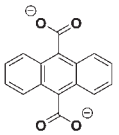

9, adc

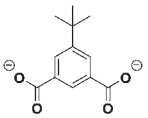

10, bbdc

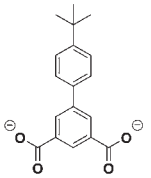

11, bbpdc

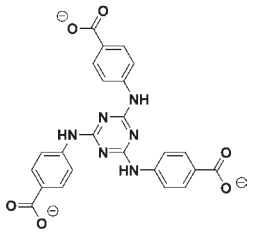

12, tatab

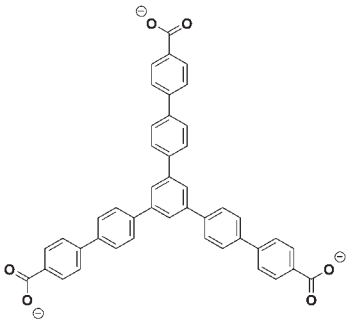

13, tcbpb

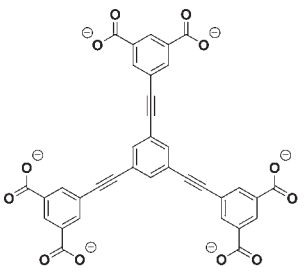

14, btei

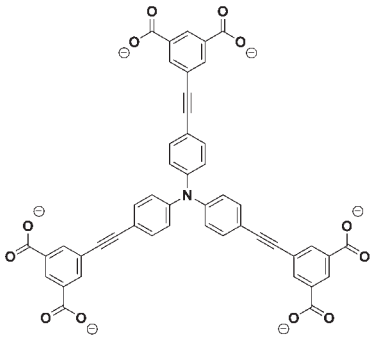

15, ntei

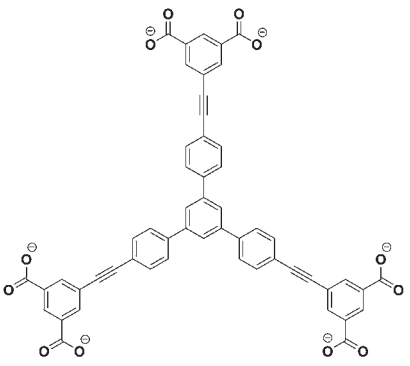

16, ptei

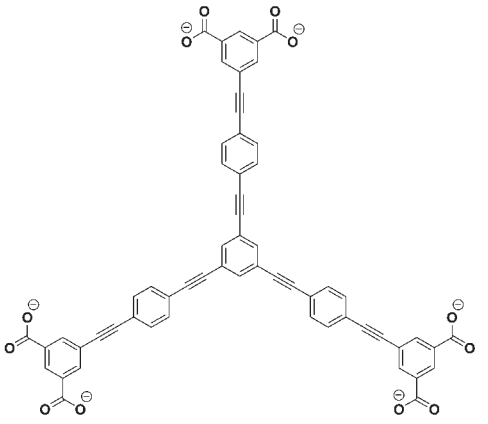

17, ttei

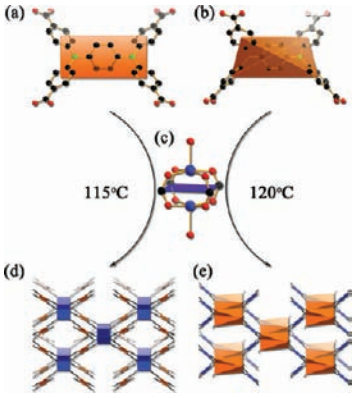

FIGURE 2. Temperature-dependent supramolecular isomerism (green, nitrogen): (a) rectangle spacer of C_{2h}-tcppda; (b) tetrahedral spacer of D_2-tcppda; (c) dicopper paddlewheel SBU as 4-linked square node; (d) NbO network; (e) PtS network.

supramolecular stereoisomerism in the generated network. A tetratopic ligand, tcppda, has been used to study this ligand-induced supramolecular isomerism in MOFs.[8] Due to the relatively free internal bond rotation around the nitrogen atoms, this ligand can adopt several different conformations. As has been identified from the crystal structure data, tcppda in the generated networks has three stereoisomers, including a diastereomer with rectangular planar C_{2h} geometry (Figure 2a) and a pair of enantiomers adopting tetrahedral D_2 geometry (Figure 2b).

The tcppda ligand adopts rectangular planar C_{2h} geometry in the NbO type network $Cu_2(C_{2h}\text{-tcppda})(H_2O)_2 \cdot 2DMSO \cdot 6H_2O$ when prepared at 115 °C. However, when the reaction is carried out at 120 °C, the crystallized product has the same formula but with the tcppda ligand adopting a tetrahedral D_2 geometry leading to a PtS type network. Conversion of the NbO network to the PtS network at higher temperatures failed, and this indicates that higher energy is required for the inversion of the N-centered propeller in a solid-state lattice than in solution. To the best of our knowledge, this is the first example of temperature-dependent supramolecular stereoisomerism.

4. Network Chirality

Porous chiral networks attract a lot of attention due to their potential application in enantioselective catalysis and separation. Current research focuses on two approaches: *induced chirality* and *intrinsic chirality*. The *induced chirality* originates from chiral ligands that retain their chirality within the network. For example, in the tcppda ligand introduced above, the rotation direction of the N-centered propellers can produce right handed ($^{\delta}D_2$) or left handed ($^{\lambda}D_2$) enantiomers. If the network is composed purely by one of these enantiomers, a chiral network will be generated. This scenario was

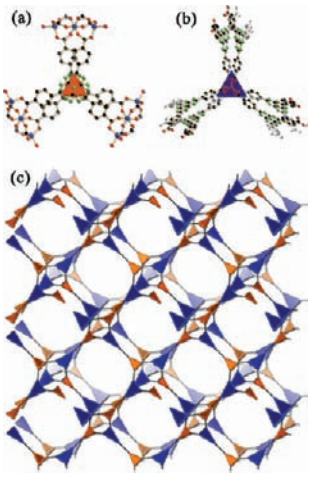

FIGURE 3. Intrinsic chirality from 3-connected spacers and nodes: (a) dimer of htb as D_3-PU spacer; (b) trinuclear hourglass SBU with htb as 3-connected node; (c) the chiral (10,3)-a network.

achieved in the zinc compound $[Zn_4O(D_2\text{-tcppda})_{1.5}] \cdot DMF \cdot H_2O$.[9] Although the bulk sample is racemic, each individual crystal is chiral with the ligand in the form of either all $^{\delta}D_2$ or all $^{\lambda}D_2$. The zinc adopts the well-known $Zn_4O(O_2CR)_6$ tetranuclear octahedron SBU (5 in Figure 1) which when linked with the enantiomerically pure tetrahedral ligand spacer generates the (6,4)-connected corundum type network. High thermal stability (stable up to 410 °C) and high porosity (Langmuir surface area of 2095 m^2/g) result.

This *induced chirality* approach is the only reliable route thus far for achieving chiral MOFs in bulk. However, it requires heavy synthetic work to prepare the chiral ligands. Scale up is often not easy and ligand racemization is always a risk during network construction. The *intrinsic chirality* approach recognizes that networks with a lack of an improper rotational axis of any order can be formed without chiral ligands. These intrinsically chiral networks are much easier to scale up and have received a lot of attention. For example, the (10,3)-a network is one of the default networks composed of 3-connected nodes and spacers, and gains its chirality from the net construction. In our group, we have synthesized two tritopic ligands as the 3-connected spacer and systematically studied the chirality, stability, and porosity of the generated (10,3)-a networks.

One of the tritopic ligands, htb, dimerizes due to strong $\pi-\pi$ stacking interactions.[10] Based on the crystal data of the solvothermal reaction product $Zn_3(htb)_2(H_2O)_2 \cdot 3DMA \cdot 5H_2O$, the dimer htb pair can be viewed as a D_3 symmetric Piedfort unit spacer (D_3-PU) which forms the (10,3)-a chiral network (Figure 3) when linked with the 3-connected trinuclear Zn hourglass SBU (2 in Figure 1). This network collapsed upon

the removal of guest molecules, preventing the further exploration of its inner space. In order to stabilize the (10,3)-a chiral network, a shorter tritopic ligand, tatb, was adopted.[11] Like htb, tatb also exists as a dimer due to strong $\pi-\pi$ interactions and functions as a D_3-PU in the new (10,3)-a network. This zinc compound, $Zn_3(tatb)_2(H_2O)_2\cdot 4DMF\cdot 6H_2O$, is stable after the removal of guest molecules and has a Langmuir surface area of 1100 m^2/g.

It needs to be emphasized that the *intrinsic chirality* approach almost always ends up with a racemic conglomerate, which is not practically applicable toward chiral separation or catalysis.[12] Rosseinsky's group has reported a series of bulk homochiral microporous MOFs with a distorted (10,3)-a network.[13] Their homochirality comes from the preferential binding of chiral auxiliary diols toward the metal center. This realization of homochiral materials in bulk through chiral auxiliary ligand binding makes the *intrinsic chirality* approach promising in enantioselective chemistry.

5. Gas Storage

Microporous materials (pore sizes within 2 nm) exhibit strong interactions with gas molecules, making them good gas sponges. Due to their tunable pore geometry and flexible network, MOFs have received growing attention in gas storage. Our group's gas storage research focuses on hydrogen and methane.

5.1. Hydrogen Storage. Hydrogen is an ideal energy carrier. However, due to its relatively inert chemical properties and extremely low critical point (32.97 K), efficient storage remains a bottleneck for the upcoming hydrogen economy. The U.S. Department of Energy (DOE) has set gravimetric and volumetric storage targets for on-board hydrogen storage for 2010 (4.5 wt %, 28 g/L) and 2015 (5.5 wt %, 40 g/L).[14] Hydrogen storage in MOFs shows great potential because of attractive kinetics and reversibility.[15,16] Under cryogenic conditions (77 K), some MOFs' hydrogen uptake capacity has reached or even surpassed the DOE target. However, at ambient temperatures, the capacity drops down dramatically. Theoretical study indicates that ambient temperature storage of hydrogen and subsequent delivery at pressures between 30 and 1.5 bar require an average adsorption enthalpy change of 15.1 kJ/mol.[17] In MOF systems, however, this enthalpy change rarely exceeds 10 kJ/mol.[15] Thus, the work of hydrogen storage in our group focuses on enhancing the interaction between hydrogen and MOFs.

The availability of coordinatively unsaturated metal centers (UMCs) in MOFs offers an approach to increase this interaction.[18] Among those SBUs that possess potential UMCs, we focus on the dinuclear copper paddlewheel, mainly due to its stability and ease of formation. One of the cases is the double-interpenetrated twist boracite type network $Cu_3(tatb)_2(H_2O)_3\cdot 11H_2O\cdot 3DMSO$ (PCN-6, PCN stands for porous coordination network).[19] At 760 Torr and 77 K, the hydrogen uptake capacity is 1.9 wt %, and we attribute this high hydrogen uptake capacity to the presence of accessible UMCs and the existence of pores and channels in a size range well-suited to the dihydrogen molecule.

In the above PCN-6 case, the interpenetration may also contribute to the enhanced hydrogen uptake capacity by narrowing down the pore and channel sizes. In order to verify that, PCN-6′ ($Cu_6(H_2O)_6(tatb)_4\cdot DMA\cdot 12H_2O$), the noninterpenetrated counterpart of PCN-6, was prepared.[20] Comparison of the gas sorption data between these two compounds allows the conclusion that interpenetration leads to a 133% of enhancement in volumetric hydrogen uptake (29% in gravimetric). The subsequent high pressure hydrogen sorption experiment confirms the beneficial effect of interpenetration in high pressure range at both cryogenic and ambient conditions (6.7 wt % at 77 K/50 bar or 0.92 wt % at 298 K/50 bar in PCN-6 vs 4.0 wt % at 77 K/50 bar or 0.40 wt % at 298 K/50 bar in PCN-6′).[21] Inelastic neutron scattering (INS) studies reveal that the UMCs are the initial sites occupied by adsorbed hydrogen, with comparable interaction energies in both PCN-6 and PCN-6′. At high hydrogen loading where the hydrogen molecules adsorb mainly on or around the organic linkers, PCN-6 exhibits a much higher hydrogen uptake indicating a substantially stronger interaction in the interpenetrated PCN-6 than in the noninterpenetrated PCN-6′ (Figure 4). PCN-6 and PCN-6′ represent the first examples of the impact of catenation supramolecular isomerism on MOFs' hydrogen uptake capacity.

PCN-20 ($Cu_2(ttca)_{4/3}(H_2O)_2\cdot 8DMF\cdot 6H_2O$) is another case where the dicopper paddlewheel SBU was included into the same twisted boracite network.[22] Compared to tatb in PCN-6′, ttca in PCN-20 has two properties that could lead to higher hydrogen uptake capacity: (1) it is smaller, which leads to shrunken pore size with higher hydrogen affinity; (2) it has highly conjugated fused triphenylene ring, which can provide more hydrogen sorption sites. Our speculation was confirmed by its hydrogen sorption data, which are much higher than those of PCN-6′ under the same conditions: 2.1 wt % (excess) at 1 bar, 77 K and 6.2 wt % (excess) at 50 bar, 77 K.

PCN-10 ($Cu_2(aobtc)(H_2O)_2\cdot 3DMA$) and PCN-11 ($Cu_2(sbtc)(H_2O)_2\cdot 3DMA$) are also MOFs containing dinuclear copper

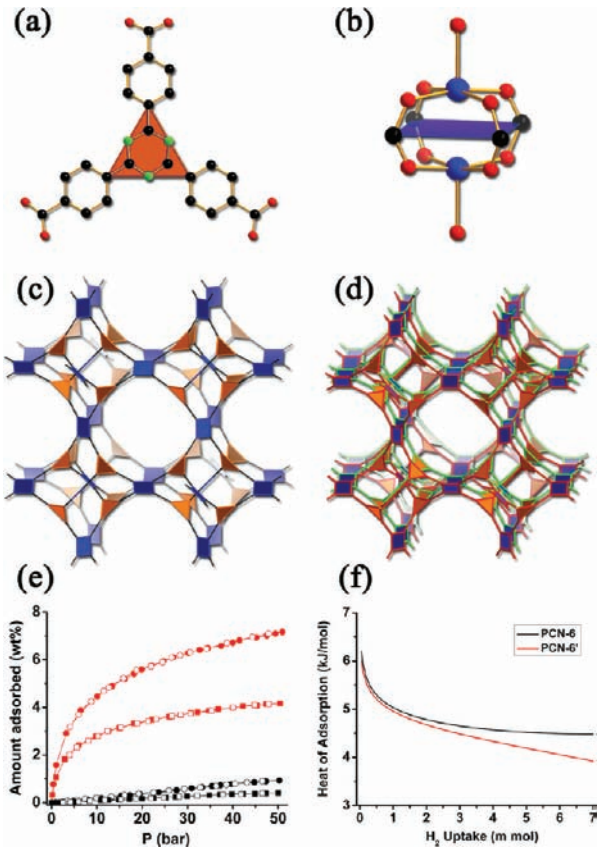

FIGURE 4. Catenation supramolecular isomerism and its impact on H_2 uptake: (a) tatb as a 3-connected spacer; (b) dinuclear copper paddlewheel as a 4-connected node; (c) twisted boracite network in PCN-6′; (d) double-interpenetrated twisted boracite network in PCN-6; (e) excess H_2 sorption isotherms of PCN-6 and PCN-6′ at 77 (red) and 298 K (black): circles, PCN-6; squares, PCN-6′; solid symbols, adsorption; open symbols, desorption; (f) isosteric heats of adsorption for PCN-6 and PCN-6′.

paddlewheel SBUs, but are constructed with tetratopic carboxylate ligands as 4-connected spacers to form the NbO type network.[23] At 760 Torr and 77 K, the hydrogen uptake capacity for PCN-10 is 2.34 wt % (18.0 g/L) and for PCN-11 is 2.55 wt % (19.1 g/L). The 77 K high pressure (~20 atm) excess hydrogen uptake capacity was also determined for PCN-10 (4.33 wt %, 33.2 g/L) and PCN-11 (5.05 wt %, 37.8 g/L). These data are consistent with the surface area difference and support the idea that surface area becomes a critical factor for hydrogen uptake capacity at higher pressure range.[15]

The in situ formed cuboctahedron, which is composed by 24 isophthalate motifs forming the edges and 12 dinuclear copper paddlewheel SBUs occupying the vertices, is believed to be advantageous in gas storage because the gas molecules may stay kinetically and thermodynamically trapped within the polyhedra by interacting with the curvature potential wall and the open copper sites. We reason that if the network is constructed by efficiently close-packing these cuboctahedra in 3D space, a stronger interaction with the gas molecules may be achieved. This "close-packing" strategy is realized by the use of a slightly different tetratopic ligand, mdip, which is composed of two isophthalate moieties linked by a bent methylene bridge.[24] Solvothermal reactions between mdip and copper salts at different temperatures (85 °C vs 120 °C) yield two Cu-mdip MOF polymorphs: PCN-12 ($[Cu_6(C_s\text{-mdip})_2(C_{2v}\text{-mdip})(H_2O)_6]\cdot 3DMA\cdot 6H_2O$) and PCN-12′ ($[Cu_2(C_{2v}\text{-mdip})(H_2O)_2]\cdot 3DMSO$). Due to the free bond rotation in the methylene group, mdip adopts both C_s and C_{2v} symmetry in PCN-12 while only C_{2v} in PCN-12′. As a result, PCN-12 is composed of cuboctahedra (a MOF with the same network geometry based on the cross-linking of cuboctahedra was reported by Zaworotko's group[25]), while PCN-12′ is not (Figure 5). The impact of close-packing cuboctahedra on hydrogen uptake capacity is impressive: 3.05 wt % (PCN-12) versus 2.40 wt % (PCN-12′), 77 K/760 Torr. To our knowledge, PCN-12 possesses the highest hydrogen uptake reported so far for MOFs at 77 K/760 Torr. The subsequent INS studies indicate that the interaction of H_2 with the open Cu sites in PCN-12 is much stronger than the interaction in HKUST-1, where only part of the UMCs are properly aligned.

Other systems also contain UMCs, one of which is PCN-9 ($H_2[Co_4O(tatb)_{8/3}]$), where the (8,3)-network is formed by linking 8-connected Co tetranuclear cuboid SBUs (4 in Figure 1) with the 3-connected spacer tatb.[26] The Co geometry within this SBU is reminiscent of the entatic state in hemoglobin/VB_{12}-like Co centers, and its high affinity toward gas molecules is supported by the following heat of adsorption data: 17.8 kJ/mol for O_2, 21.0 kJ/mol for CO, 10.1 kJ/mol for H_2, and 23.3 kJ/mol for CH_4. In the succedent research, entatic Fe and Mn centers were also included into MOFs with the same geometry: PCN-9 (Fe) ($Fe_4O(tatb)_{8/3}\cdot 5H_2O\cdot 10DMSO$) and PCN-9 (Mn) ($Mn_4O(tatb)_{8/3}\cdot 2H_3O^+\cdot 5H_2O\cdot 8DMSO$).[27] The entatic Co center has the highest affinity to hydrogen, while entatic Fe has the lowest. This affinity difference is in accordance with the metals' coordination preferences, while the relatively lower heat of adsorption for Fe is attributed to the partial oxidation of Fe^{2+} to Fe^{3+}.

5.2. Methane Storage. Methane is another good candidate for on-board fuel, but it also lacks an effective storage method. Unlike hydrogen storage where the low heat of adsorption is the bottleneck, the heat of adsorption for methane is already within the ideal scope to be applicable under ambient conditions.[28] Since the DOE methane storage target is based on volumetric density (180 v/v, at

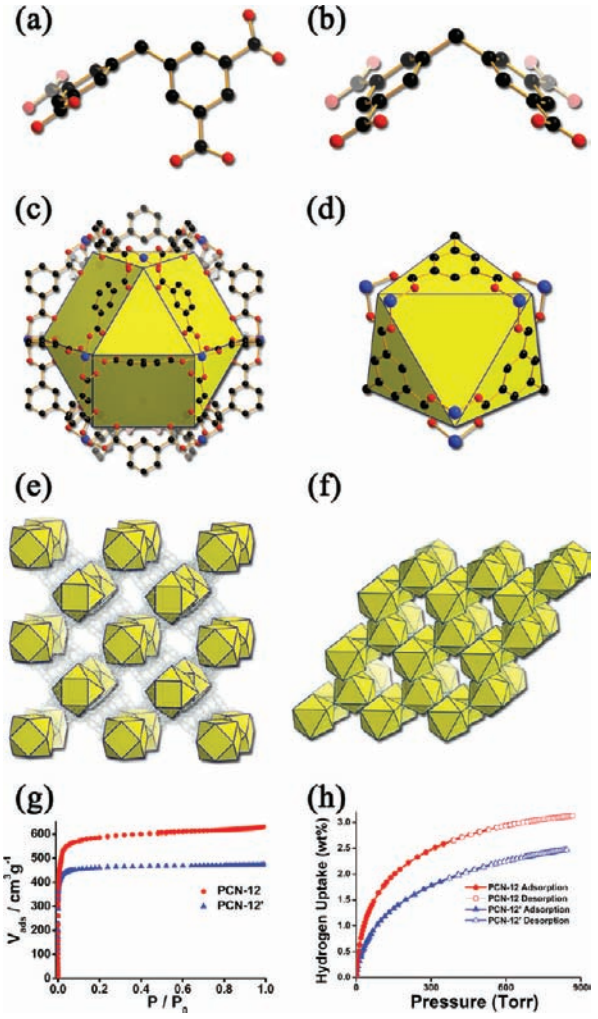

FIGURE 5. UMCs alignment and close-packing strategy toward high H_2 uptake: (a) mdip with C_s conformation; (b) mdip with C_{2v} conformation; (c) a cuboctahedral cage in PCN-12; (d) a tricapped trigonal prismatic cage in PCN-12′; (e) cuboctahedron packing in PCN-12; (f) tricapped trigonal prismatic cage packing in PCN-12′; (g) N_2 adsorption isotherms for PCN-12 (red) and PCN-12′ (blue); (h) H_2 adsorption isotherms for PCN-12 (red) and PCN-12′ (blue).

ambient conditions within 35 bar), the high packing density of the adsorbent should be the working direction.[29]

The aforementioned PCN-11 has been tested for its methane uptake capacity.[23] For application at 298 K and 35 bar, the excess uptake of methane for PCN-11 is 171 v/v, which is very close to the DOE target and demonstrates the potential application of MOFs in methane storage. The real breakthrough for MOF-based methane storage is achieved in PCN-14 ($Cu_2(H_2O)_2(adip)\cdot 2DMF$).[30] At 290 K and 35 bar, the absolute methane adsorption capacity in PCN-14 is 230 v/v, which is 28% higher than the DOE target (Figure 6). The heat of adsorption at low loading is as high as 30 kJ/mol, indicating strong interactions between methane and the

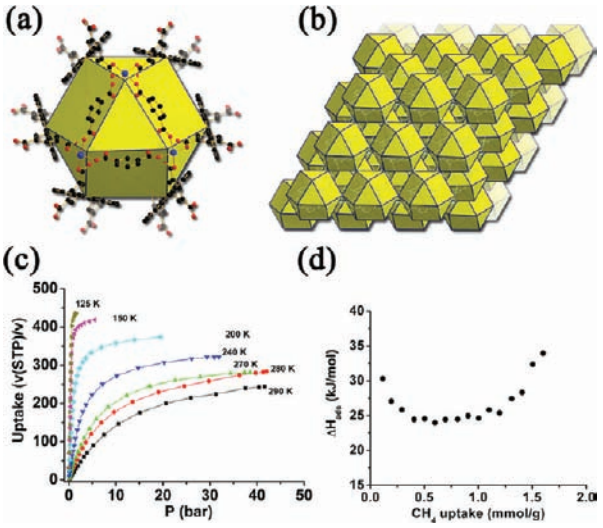

FIGURE 6. Squashed cuboctahedron packing and methane uptake in PCN-14: (a) a squashed cuboctahedral cage in PCN-14; (b) 3D polyhedron packing; (c) high-pressure methane absolute sorption isotherms at various temperatures; (d) isosteric heats of adsorption of methane.

network. This incredibly high methane uptake capacity may come from (1) the ligand adip, which is derived from anthracene with an extended π system and stronger gas interaction; (2) the NbO type network constructed from the squashed cuboctahedral cages that can trap gas; (3) the relatively high crystal density.

6. Selective Gas Adsorption

Gas separation plays an important role in industry. The traditional methods, such as distillation and absorption, suffer from huge energy consumption and environmental pollution. By using molecular sieves with pore sizes comparable to the gas molecules, gas separation can be achieved in an energy-conserving and environmentally friendly approach. During this process, the ability of the sorbent to selectively adsorb different gases is always the prerequisite. MOFs have the advantages of tunable pore sizes and flexible structure, which make them good candidates for efficient and versatile selective gas adsorption.[31] Our lab develops several strategies to tune the pore size of MOFs so that they can match up with the size of the gases being separated to achieve selective adsorption.

Our first approach is using bulky ligand, a case of which is the bulky ligand adc in PCN-13 ($Zn_4O(H_2O)_3(adc)_3\cdot DMF$).[32] As anticipated, the pore size is dramatically reduced to less than 4 Å. As a result, PCN-13 can uptake a large amount of H_2 (kinetic diameter: 2.89 Å) and O_2 (kinetic diameter: 3.46 Å), but only a very limited amount of the larger gases N_2 (kinetic diameter: 3.64 Å) and CO (kinetic diameter: 3.76 Å). Given

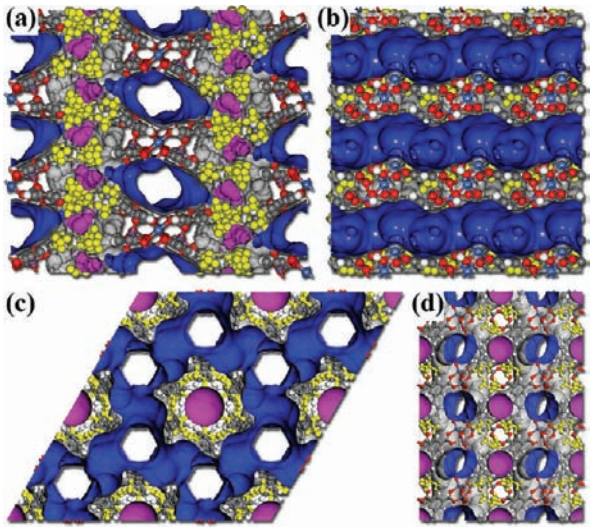

FIGURE 7. Atomic packing in activated MAMS (blue, hydrophilic channel; pink, hydrophobic chamber; yellow, *t*-butyl group): (a) MAMS-1, viewed along the [1 0 0] direction; (b) MAMS-1, viewed along the [0 0 1] direction; (c) MAMS-2, viewed along the [0 0 1] direction; (d) MAMS-2, viewed along the [1 0 0] direction.

the sizes of the gases, the pore size of PCN-13 should be between 3.46 and 3.64 Å, which is consistent with the crystal data.

Network interpenetration offers another option toward reduced pore size. In PCN-5 ($H_2[Ni_3O(H_2O)_3(tatb)_2]\cdot 5DMF\cdot 2H_2O$), 3-connected tatb spacers are linked to trinuclear nickel prism SBUs (3 in Figure 1) to form a double-interpenetrated (3,6)-network.[33] The interpenetration is probably responsible for the notable hysteresis seen in each of the N_2 and H_2 isotherms. Considering the pore size openings of about 3.3 Å in PCN-5, the selective adsorption of CO_2 (3.3 Å) over CH_4 (3.8 Å) can also be contributed to the molecular-sieving effect. In addition, a series of double-interpenetrated MOFs (PCN-17) have been prepared from the lanthanide ions Dy, Y, Er, and Yb, and the network geometry is reminiscent of PCN-9. The pore sizes are 3.46−3.64 Å for PCN-17 (Yb) and ~3.7 Å for the rest. They are restricted by the linking of open sites of the tetranuclear cuboid SBUs with in situ generated SO_4^{2-}.[34,35] The crystal units shrink in the order of Dy, Y, Er, and Yb, which is consistent with lanthanide contraction. Each shows selective adsorption of H_2 (2.89 Å) and O_2 (3.46 Å) over N_2 (3.64 Å) and CO (3.76 Å).

In the cases above, the reduced pore sizes are relatively fixed. If the pore size could be tuned continuously by external stimuli, a wider variety of gases could be selectively adsorbed. This dynamic selective gas adsorption has been achieved in our group with MAMS-1 (Ni_8(5-bbdc)$_6(\mu_3$-OH)$_4$) (MAMS stands for mesh adjustable molecule sieves).[36] This

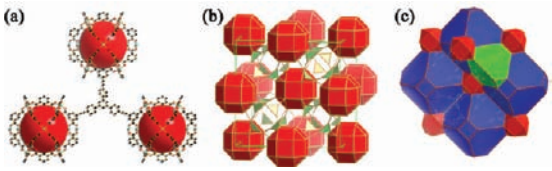

FIGURE 8. Framework topology in PCN-68: (a) cuboctahedra as structural building units; (b) (3,24)-connected network; (c) 3D polyhedra packing.

stacked 2D layer structure is composed of an amphiphilic ligand bbdc linked to an octanickel cluster. This network contains both a hydrophilic channel—which is formed after activation and has very limited gas accommodation capacity—and a hydrophobic chamber which serves as the primary gas reservoir (Figure 7a, b). During the sorption process, gases are first adsorbed into the hydrophilic channel and then enter the hydrophobic chamber through gates formed by *t*-butyl groups. At lower temperatures, the opening of the gate is limited due to the partial freezing of the *t*-butyl group. While at higher temperatures, the more intense thermal vibration of the *t*-butyl group leads to a larger gate opening, and a greater amount of gas can enter the hydrophobic chamber. The adsorption data at varied temperatures with different gases indicate that the gate opening can be continually changed from 2.9 to 5.0 Å, allowing effective separations between H_2/N_2, H_2/CO, N_2/O_2, N_2/CH_4, CH_4/C_2H_4, and C_2H_4/C_3H_6 at different temperatures. More MAMS materials, MAMS-2 ($Zn_2(H_2O)_2(bbpdc)_2\cdot 3DMF$), MAMS-3 ($Co_2(H_2O)_2(bbpdc)_2\cdot 3DMA$), and MAMS-4 ($Cu_2(H_2O)_2(bbpdc)_2\cdot 3DMF$), have been synthesized with a common structure.[37] In these series of compounds, a longer amphiphilic ligand bbpdc was used, and the hydrophobic cage was formed by surrounding three bbpdc ligands (Figure 7c, d). Like MAMS-1, these materials also demonstrate selective gas adsorption property at different temperatures. A further exploration of the gas sorption data reveals a linear relationship between mesh size and temperature, $D = D_0 + \alpha T$ (D, mesh size at temperature T K; D_0, mesh size at 0 K; α, constant). The constants D_0 and α are only relevant to the ligand structure, while independent of the metals adopted.

7. Network Stabilization

Porosity is the main property distinguishing MOFs from other solid state materials. There is a growing interest in building MOFs with larger pores, because in some applications, such as catalysis, a larger pore is the prerequisite for the accommodation of large guest molecules.[38] Although pore size can be increased by ligand extension, reduced network stability typically results. Careful consideration of porosity versus stability must be taken.

TABLE 1. Functionality of Selected MOFs in Zhou's Group

MOFs	metal SBU	network geometry	network functionality	ref
$Cu_2(D_2$-tcppda$)(H_2O)_2\cdot 2DMSO\cdot 6H_2O$	dinuclear paddlewheel	PtS	thermosensitive supramolecular stereoisomers, permanent porosity	8
$Cu_2(C_{2h}$-tcppda$)(H_2O)_2\cdot 2DMSO\cdot 6H_2O$	dinuclear paddlewheel	NbO	thermosensitive supramolecular stereoisomers, permanent porosity	8
$[Zn_4O(D_2$-tcppda$)_{1.5}]\cdot DMF\cdot H_2O$	tetranuclear octahedron	corundum	chiral network, permanent porosity	9
Zn_3(htb$)_2(H_2O)_2\cdot 3DMA\cdot 5H_2O$	trinuclear hourglass	(10,3)-a	chiral network	10
Zn_3(tatb$)_2(H_2O)_2\cdot 4DMF\cdot 6H_2O$	trinuclear hourglass	(10,3)-a	chiral network, permanent porosity	11
Cu_3(tatb$)_2(H_2O)_3\cdot 11H_2O\cdot 3DMSO$, PCN-6	dinuclear paddlewheel	double-interpenetrated twisted boracite	permanent porosity, high hydrogen uptake capacity	19,21
$Cu_6(H_2O)_6$(tatb$)_4\cdot DMA\cdot 12H_2O$, PCN-6′	dinuclear paddlewheel	twisted boracite	permanent porosity, moderate hydrogen uptake capacity, catenation supramolecular isomer with PCN-6	20,21
Cu_2(ttca$)_{4/3}(H_2O)_2\cdot 8DMF\cdot 6H_2O$, PCN-20	dinuclear paddlewheel	twisted boracite	permanent porosity, high hydrogen uptake capacity	22
Cu_2(aobtc$)(H_2O)_2\cdot 3DMA$, PCN-10	dinuclear paddlewheel	NbO	permanent porosity, high hydrogen and methane uptake capacity	23
Cu_2(sbtc$)(H_2O)_2\cdot 3DMA$, PCN-11	dinuclear paddlewheel	NbO	permanent porosity, high hydrogen and methane uptake capacity	23
$[Cu_6(C_s$-mdip$)_2(C_{2v}$-mdip$)(H_2O)_6]\cdot$ 3DMA·6H2O, PCN-12	dinuclear paddlewheel		permanent porosity, high hydrogen uptake capacity	24
$[Cu_2(C_{2v}$-mdip$)(H_2O)_2]\cdot 3DMSO$, PCN-12′	dinuclear paddlewheel		permanent porosity, moderate hydrogen uptake capacity, supramolecular stereoisomer with PCN-12	24
$H_2[Co_4O$(tatb$)_{8/3}]$, PCN-9	tetranuclear cuboid	double-interpenetrated (8−3)-net	permanent porosity, entatic metal centers, high gas adsorption affinity	26
$Cu_2(H_2O)_2$(adip$)\cdot 2DMF$, PCN-14	dinuclear paddlewheel	NbO	permanent porosity, high methane uptake capacity	30
$Zn_4O(H_2O)_3$(adc$)_3\cdot DMF$, PCN-13	distorted tetranuclear octahedron		reduced pore size, selective adsorption of H_2 and O_2 over N_2 and CO	32
$H_2[Ni_3O(H_2O)_3$(tatb$)_2]\cdot 5DMF\cdot$ $2H_2O$, PCN-5	trinuclear prism	double-interpenetrated (3,6)-net	reduced pore size, selective adsorption of CO_2 over CH_4, pronounced gas-sorption hysteresis	33
$Yb_4(\mu_4H_2O)$(tatb$)_{8/3}(SO_4)_2\cdot 3H_2O\cdot$ 10DMSO, PCN-17 (Yb)	tetranuclear cuboid	double-interpenetrated (8−3)-net	high thermal stability, reduced pore size, selective adsorption of H_2 and O_2 over N_2 and CO	34,35
Ni_8(5-bbdc$)_6(\mu_3$-OH$)_4$, MAMS-1		stacked 2D layer	from 2.9 to 5.0 Å thermally adjustable pore size, selective adsorption of gases with different sizes at different temperatures	36,37
$Zn_2(H_2O)_2$(bbpdc$)_2\cdot 3DMF$, MAMS-2		stacked 2D layer	from 2.9 to 5.0 Å thermally adjustable pore size, selective adsorption of gases with different sizes at different temperatures	36,37
$Co_2(H_2O)_2$(bbpdc$)_2\cdot 3DMA$, MAMS-3		stacked 2D layer	from 2.9 to 5.0 Å thermally adjustable pore size, selective adsorption of gases with different sizes at different temperatures	36,37
$Cu_2(H_2O)_2$(bbpdc$)_2\cdot 3DMF$, MAMS-4		stacked 2D layer	from 2.9 to 5.0 Å thermally adjustable pore size, selective adsorption of gases with different sizes at different temperatures	36,37
Cu_3(tatab$)_2(H_2O)_3\cdot 8DMF\cdot 9H_2O$, mesoMOF-1	dinuclear paddlewheel	twisted boracite	composed by nanoscopic ligand, permanent mesoporosity with type IV isotherms after being stabilized by postsynthesis neutralization	39
Mn_6O(tatb$)_4\cdot(H^+)_2\cdot(H_2O)_8\cdot(DMF)_2$	trinuclear hourglass		high thermal stability, strong $\pi-\pi$ stacking	40
$Zn_8(OH)_4$(tcbpb$)_4\cdot 2DMF\cdot EtOH\cdot 3H_2O$			composed by nanoscopic ligand, permanent porosity	41
$[Cu(H_2O)]_3$(btei$)\cdot 5DMF\cdot 4H_2O$, PCN-61	dinuclear paddlewheel	(3,24)-connected network	permanent porosity, high gas uptake capacity	42,43
$[Cu(H_2O)]_3$(ntei$)\cdot 21DMA\cdot 10H_2O$, PCN-66	dinuclear paddlewheel	(3,24)-connected network	permanent porosity, high gas uptake capacity	42,43
$[Cu(H_2O)]_3$(ptei$)\cdot 33DMF\cdot 13H_2O$, PCN-68	dinuclear paddlewheel	(3,24)-connected network	permanent porosity, high gas uptake capacity	42,43
$[Cu(H_2O)_3]$(ttei$)\cdot 22DMF\cdot 19H_2O$, PCN-610	dinuclear paddlewheel	(3,24)-connected network	permanent porosity, high gas uptake capacity	42,43

The organic ligand can be used to help stabilize the networks. For example, mesoMOF-1 (Cu_3(tatab$)_2(H_2O)_3\cdot$ $8DMF\cdot 9H_2O$) has a large pore size and loses solvent quickly once taken out from the mother liquor.[39] This neutral network can be turned ionic by treating the amine group in the ligand with acid. The resulting electronic repulsion keeps the network from collapsing and gives rise to the first case of a mesoporous MOF that demonstrates the type IV isotherm. In another example, the $\pi-\pi$ stacking interaction between parallel tatb ligands was used to strengthen the organic spacer. By linking the tatb dimer with infinite trinuclear hourglass SBUs (Mn, Co, and Zn), a series of MOFs with high

thermal stability were obtained.[40] In one of the MOFs, $Mn_6O(tatb)_4 \cdot (H^+)_2 \cdot (H_2O)_8 \cdot (DMF)_2$, the distance between the centers of the two triazine rings is only 3.5 Å and may be the strongest $\pi-\pi$ stacking observed. This dimerization strengthens the pore wall and enables the MOF to remain stable up to 400 °C, among the highest reported.

By solidifying the inorganic building nodes, the networks can also be stabilized accordingly. In the tatb case just mentioned, the hourglass SBUs are linked together to form a tetrahedral network, which also contributes to high thermal stability. In the case of the PCN-17 series, high thermal stability (up to 500 °C) was achieved by interlinking all the SBUs with SO_4^{2-}.[34,35] Our first attempt in using the nanoscopic ligand tcbpb to build a MOF resulted in a collapsed network upon solvent removal.[41] In order to stabilize this network, a noncoordinating base was used to eliminate binding labile terminal ligands in the SBU ($Zn_8(OH)_4(tcbpb)_4 \cdot 2DMF \cdot EtOH \cdot 3H_2O$). The network generated under these conditions is stable up to 400 °C in an inert atmosphere with permanent porosity and a Langmuir surface area of 942 m^2/g.

Last but not least, judicious choice of the topology would also help to stabilize the network. PCN-61 ($[Cu(H_2O)]_3(btei) \cdot 5DMF \cdot 4H_2O$), PCN-66 ($[Cu(H_2O)]_3(ntei) \cdot 21DMA \cdot 10H_2O$), PCN-68 ($[Cu(H_2O)]_3(ptei) \cdot 33DMF \cdot 13H_2O$), and PCN-610 ($[Cu(H_2O)_3](ttei) \cdot 22DMF \cdot 19H_2O$) are isoreticular MOFs constructed by nanoscopic ligands with the same (3,24)-connected network topology.[42,43] Generally speaking, MOFs based on nanoscopic ligands tend to collapse upon vacuation, because the large void derived from the long ligand is not stable after the removal of guest molecules. In the cases of PCN-61, PCN-66, PCN-68, and PCN-610, the aforementioned cuboctahedral cage serves as building unit in the (3,24)-connected network topology (Figure 8). They narrow down the opening of the mesocavities into microwindows and contribute to the stability of the MOFs. As a result, three of them (PCN-61, PCN-66, and PCN-68) demonstrate permanent porosity, with one of them (PCN-68, also been reported as NOTT-116 by Schröder's group[44]) having a surface area that is among the highest in all of the MOFs reported (Langmuir surface area, 6033 m^2/g; BET surface area, 5109 m^2/g). At 77 K, the gravimetric excess hydrogen uptake capacity in PCN-68 can reach 6.82 wt %, also among the highest been reported.

8. Outlook

In retrospect, beside geometric certainty and diversity, other properties of organic ligands, such as size, amphiphilicity, dimerization, isomerism, and functional groups suitable for postsynthesis chemical modification, contribute to the characters of the generated networks and enrich their functionality (Table 1). Despite the abundant achievements in the MOF field worldwide, there is still much room for further exploration. We will be continuing our efforts and look forward to contributing to this blossoming field in the next decade.

This work was supported by the U.S. Department of Energy (DE-FC36-07GO17033, hydrogen storage; DE-SC0001015, selective gas adsorption), the National Science Foundation (CHE-0930079), and the Welch Foundation (A-1706).

BIOGRAPHICAL INFORMATION

Dan Zhao received his B.S. (2003) and M.S. (2006) in Polymer Chemistry & Physics from Zhejiang University, and his Ph.D. (2010) in Inorganic Chemistry from Texas A&M University under the supervision of Professor Hong-Cai Zhou. His research interests include metal−organic materials and their applications in clean and renewable energy field.

Daren J. Timmons received his B.S. from Duke University (1994) and Ph.D. from Texas A&M University (1999) with Professor F. Albert Cotton, and he was a Postdoctoral Associate with Professor Michael P. Doyle (1999−2001) at the University of Arizona. He is currently an Associate Professor of Chemistry at the Virginia Military Institute and recently finished a sabbatical in Professor Hong-Cai Zhou's laboratory. He has several research directions centered on flavonoids and works almost exclusively with undergraduate students on self-organized and self-assembled materials.

Daqiang Yuan received his B.S. (1999) and M.S. (2002) from Beijing Normal University, and his Ph.D. (2006) in Physical Chemistry from Fujian Institute of Research on the Structure of Matter, Chinese Academy of Sciences under the supervision of Professor Maochun Hong. Since then, he has been working as a Research Assistant in Prof. Maochun Hong's group. He joined Professor Hong-Cai Zhou's group as a Postdoctoral Associate (2007 until now). His research interests include the rational design and synthesis of metal−organic frameworks and their application in gas storage.

Hong-Cai "Joe" Zhou obtained his Ph.D. in 2000 from Texas A&M University under the supervision of F. A. Cotton. After a postdoctoral stint at Harvard University with R. H. Holm, he joined the faculty of Miami University, Oxford in 2002. Since the fall of 2008, he has been a professor of chemistry at Texas A&M University. His research interest focuses on hydrogen/methane storage and gas separation that are relevant to clean energy technologies.

FOOTNOTES

*To whom correspondence should be addressed. E-mail: zhou@mail.chem.tamu.edu.

REFERENCES

1 Férey, G. Hybrid Porous Solids: Past, Present, Future. *Chem. Soc. Rev.* **2008**, *37*, 191–214.
2 Kitagawa, S.; Kitaura, R.; Noro, S. Functional Porous Coordination Polymers. *Angew. Chem., Int. Ed.* **2004**, *43*, 2334–2375.

3 Yaghi, O. M.; O'Keeffe, M.; Ockwig, N. W.; Chae, H. K.; Eddaoudi, M.; Kim, J. Reticular Synthesis and the Design of New Materials. *Nature* **2003**, *423*, 705–714.

4 O'Keeffe, M.; Peskov, M. A.; Ramsden, S. J.; Yaghi, O. M. The Reticular Chemistry Structure Resource (RCSR) Database of, and Symbols for, Crystal Nets. *Acc. Chem. Res.* **2008**, *41*, 1782–1789.

5 Eddaoudi, M.; Moler, D. B.; Li, H. L.; Chen, B. L.; Reineke, T. M.; O'Keeffe, M.; Yaghi, O. M. Modular Chemistry: Secondary Building Units as a Basis for the Design of Highly Porous and Robust Metal-Organic Carboxylate Frameworks. *Acc. Chem. Res.* **2001**, *34*, 319–330.

6 de Meijere, A.; Diederich, F. *Metal-Catalyzed Cross-Coupling Reactions*; Wiley-VCH: Weinheim, 2004.

7 Moulton, B.; Zaworotko, M. J. From Molecules to Crystal Engineering: Supramolecular Isomerism and Polymorphism in Network Solids. *Chem. Rev.* **2001**, *101*, 1629–1658.

8 Sun, D. F.; Ke, Y. X.; Mattox, T. M.; Ooro, B. A.; Zhou, H. C. Temperature-Dependent Supramolecular Stereoisomerism in Porous Copper Coordination Networks Based on a Designed Carboxylate Ligand. *Chem. Commun.* **2005**, *5447*, 5449.

9 Sun, D. F.; Collins, D. J.; Ke, Y. X.; Zuo, J. L.; Zhou, H. C. Construction of Open Metal-Organic Frameworks Based on Predesigned Carboxylate Isomers: From Achiral to Chiral Nets. *Chem.—Eur. J.* **2006**, *12*, 3768–3776.

10 Ke, Y. X.; Collins, D. J.; Sun, D. F.; Zhou, H. C. (10,3)-a Noninterpenetrated Network Built from a Piedfort Ligand Pair. *Inorg. Chem.* **2006**, *45*, 1897–1899.

11 Sun, D. F.; Ke, Y. X.; Collins, D. J.; Lorigan, G. A.; Zhou, H. C. Construction of Robust Open Metal-Organic Frameworks with Chiral Channels and Permanent Porosity. *Inorg. Chem.* **2007**, *46*, 2725–2734.

12 Morris, R. E.; Bu, X. H. Induction of Chiral Porous Solids Containing Only Achiral Building Blocks. *Nat. Chem.* **2010**, *2*, 353–361.

13 Kepert, C. J.; Prior, T. J.; Rosseinsky, M. J. A Versatile Family of Interconvertible Microporous Chiral Molecular Frameworks: The First Example of Ligand Control of Network Chirality. *J. Am. Chem. Soc.* **2000**, *122*, 5158–5168.

14 Yang, J.; Sudik, A.; Wolverton, C.; Siegel, D. J. High Capacity Hydrogen Storage Materials: Attributes for Automotive Applications and Techniques for Materials Discovery. *Chem. Soc. Rev.* **2010**, *39*, 656–675.

15 Zhao, D.; Yuan, D. Q.; Zhou, H. C. The Current Status of Hydrogen Storage in Metal-Organic Frameworks. *Energy Environ. Sci.* **2008**, *1*, 222–235.

16 Collins, D. J.; Zhou, H. C. Hydrogen Storage in Metal-Organic Frameworks. *J. Mater. Chem.* **2007**, *17*, 3154–3160.

17 Bhatia, S. K.; Myers, A. L. Optimum Conditions for Adsorptive Storage. *Langmuir* **2006**, *22*, 1688–1700.

18 Dincă, M.; Long, J. R. Hydrogen Storage in Microporous Metal-Organic Frameworks with Exposed Metal Sites. *Angew. Chem., Int. Ed.* **2008**, *47*, 6766–6779.

19 Sun, D. F.; Ma, S. Q.; Ke, Y. X.; Collins, D. J.; Zhou, H. C. An Interweaving MOF with High Hydrogen Uptake. *J. Am. Chem. Soc.* **2006**, *128*, 3896–3897.

20 Ma, S. Q.; Sun, D. F.; Ambrogio, M.; Fillinger, J. A.; Parkin, S.; Zhou, H. C. Framework-Catenation Isomerism in Metal-Organic Frameworks and Its Impact on Hydrogen Uptake. *J. Am. Chem. Soc.* **2007**, *129*, 1858–1859.

21 Ma, S. Q.; Eckert, J.; Forster, P. M.; Yoon, J. W.; Hwang, Y. K.; Chang, J. S.; Collier, C. D.; Parise, J. B.; Zhou, H. C. Further Investigation of the Effect of Framework Catenation on Hydrogen Uptake in Metal-Organic Frameworks. *J. Am. Chem. Soc.* **2008**, *130*, 15896–15902.

22 Wang, X. S.; Ma, S. Q.; Yuan, D. Q.; Yoon, J. W.; Hwang, Y. K.; Chang, J. S.; Wang, X. P.; Jorgensen, M. R.; Chen, Y. S.; Zhou, H. C. A Large-Surface-Area Boracite-Network-Topology Porous MOF Constructed from a Conjugated Ligand Exhibiting a High Hydrogen Uptake Capacity. *Inorg. Chem.* **2009**, *48*, 7519–7521.

23 Wang, X. S.; Ma, S. Q.; Rauch, K.; Simmons, J. M.; Yuan, D. Q.; Wang, X. P.; Yildirim, T.; Cole, W. C.; López, J. J.; de Meijere, A.; Zhou, H. C. Metal-Organic Frameworks Based on Double-Bond-Coupled Di-Isophthalate Linkers with High Hydrogen and Methane Uptakes. *Chem. Mater.* **2008**, *20*, 3145–3152.

24 Wang, X. S.; Ma, S. Q.; Forster, P. M.; Yuan, D. Q.; Eckert, J.; López, J. J.; Murphy, B. J.; Parise, J. B.; Zhou, H. C. Enhancing H_2 Uptake by "Close-Packing" Alignment of Open Copper Sites in Metal-Organic Frameworks. *Angew. Chem., Int. Ed.* **2008**, *47*, 7263–7266.

25 Perry, J. J.; Kravtsov, V. C.; McManus, G. J.; Zaworotko, M. J. Bottom up Synthesis That Does Not Start at the Bottom: Quadruple Covalent Cross-Linking of Nanoscale Faceted Polyhedra. *J. Am. Chem. Soc.* **2007**, *129*, 10076–10077.

26 Ma, S. Q.; Zhou, H. C. A Metal-Organic Framework with Entatic Metal Centers Exhibiting High Gas Adsorption Affinity. *J. Am. Chem. Soc.* **2006**, *128*, 11734–11735.

27 Ma, S. Q.; Yuan, D. Q.; Chang, J. S.; Zhou, H. C. Investigation of Gas Adsorption Performances and H_2 Affinities of Porous Metal-Organic Frameworks with Different Entatic Metal Centers. *Inorg. Chem.* **2009**, *48*, 5398–5402.

28 Menon, V. C.; Komarneni, S. Porous Adsorbents for Vehicular Natural Gas Storage: A Review. *J. Porous Mater.* **1998**, *5*, 43–58.

29 Düren, T.; Sarkisov, L.; Yaghi, O. M.; Snurr, R. Q. Design of New Materials for Methane Storage. *Langmuir* **2004**, *20*, 2683–2689.

30 Ma, S. Q.; Sun, D. F.; Simmons, J. M.; Collier, C. D.; Yuan, D. Q.; Zhou, H. C. Metal-Organic Framework from an Anthracene Derivative Containing Nanoscopic Cages Exhibiting High Methane Uptake. *J. Am. Chem. Soc.* **2008**, *130*, 1012–1016.

31 Li, J. R.; Kuppler, R. J.; Zhou, H. C. Selective Gas Adsorption and Separation in Metal-Organic Frameworks. *Chem. Soc. Rev.* **2009**, *38*, 1477–1504.

32 Ma, S. Q.; Wang, X. S.; Collier, C. D.; Manis, E. S.; Zhou, H. C. Ultramicroporous Metal-Organic Framework Based on 9,10-Anthracenedicarboxylate for Selective Gas Adsorption. *Inorg. Chem.* **2007**, *46*, 8499–8501.

33 Ma, S. Q.; Wang, X. S.; Manis, E. S.; Collier, C. D.; Zhou, H. C. Metal-Organic Framework Based on a Trinickel Secondary Building Unit Exhibiting Gas-Sorption Hysteresis. *Inorg. Chem.* **2007**, *46*, 3432–3434.

34 Ma, S. Q.; Wang, X. S.; Yuan, D. Q.; Zhou, H. C. A Coordinatively Linked Yb Metal-Organic Framework Demonstrates High Thermal Stability and Uncommon Gas-Adsorption Selectivity. *Angew. Chem., Int. Ed.* **2008**, *47*, 4130–4133.

35 Ma, S. Q.; Yuan, D. Q.; Wang, X. S.; Zhou, H. C. Microporous Lanthanide Metal-Organic Frameworks Containing Coordinatively Linked Interpenetration: Syntheses, Gas Adsorption Studies, Thermal Stability Analysis, and Photoluminescence Investigation. *Inorg. Chem.* **2009**, *48*, 2072–2077.

36 Ma, S. Q.; Sun, D. F.; Wang, X. S.; Zhou, H. C. A Mesh-Adjustable Molecular Sieve for General Use in Gas Separation. *Angew. Chem., Int. Ed.* **2007**, *46*, 2458–2462.

37 Ma, S. Q.; Sun, D. F.; Yuan, D. Q.; Wang, X. S.; Zhou, H. C. Preparation and Gas Adsorption Studies of Three Mesh-Adjustable Molecular Sieves with a Common Structure. *J. Am. Chem. Soc.* **2009**, *131*, 6445–6451.

38 Férey, G.; Mellot-Draznieks, C.; Serre, C.; Millange, F. Crystallized Frameworks with Giant Pores: Are There Limits to the Possible. *Acc. Chem. Res.* **2005**, *38*, 217–225.

39 Wang, X. S.; Ma, S. Q.; Sun, D. F.; Parkin, S.; Zhou, H. C. A Mesoporous Metal-Organic Framework with Permanent Porosity. *J. Am. Chem. Soc.* **2006**, *128*, 16474–16475.

40 Sun, D. F.; Ma, S. Q.; Ke, Y. X.; Petersen, T. M.; Zhou, H. C. Synthesis, Characterization, and Photoluminescence of Isostructural Mn, Co, and Zn MOFs Having a Diamondoid Structure with Large Tetrahedral Cages and High Thermal Stability. *Chem. Commun.* **2005**, *2663*, 2665.

41 Sun, D. F.; Ke, Y. X.; Mattox, T. M.; Parkin, S.; Zhou, H. C. Stability and Porosity Enhancement through Concurrent Ligand Extension and Secondary Building Unit Stabilization. *Inorg. Chem.* **2006**, *45*, 7566–7568.

42 Zhao, D.; Yuan, D. Q.; Sun, D. F.; Zhou, H. C. Stabilization of Metal-Organic Frameworks with High Surface Areas by the Incorporation of Mesocavities with Microwindows. *J. Am. Chem. Soc.* **2009**, *131*, 9186–9188.

43 Yuan, D. Q.; Zhao, D.; Sun, D. F.; Zhou, H. C. An Isoreticular Series of Metal-Organic Frameworks with Dendritic Hexacarboxylate Ligands and Exceptionally High Gas-Uptake Capacity. *Angew. Chem., Int. Ed.* **2010**, *49*, 5357–5361.

44 Yan, Y.; Telepeni, I.; Yang, S. H.; Lin, X.; Kockelmann, W.; Dailly, A.; Blake, A. J.; Lewis, W.; Walker, G. S.; Allan, D. R.; Barnett, S. A.; Champness, N. R.; Schröder, M. Metal-Organic Polyhedral Frameworks: High H_2 Adsorption Capacities and Neutron Powder Diffraction Studies. *J. Am. Chem. Soc.* **2010**, *132*, 4092–4094.